horticulturae

MDPI

Article

Assessing Nitrogen Fertilization in Processing Pepper: Critical Nitrogen Curve, Yield Response, and Crop Development

Jose Maria Vadillo *, Carlos Campillo, Valme González and Henar Prieto *

Center for Scientific and Technological Research of Extremadura (CICYTEX), Area of Agronomy of Woody and Horticultural Crops, Finca La Orden, Autovía A-V, km372, Guadajira, 06187 Badajoz, Spain; carlos.campillo@juntaex.es (C.C.); valme.gonzalez@juntaex.es (V.G.)

* Correspondence: josemaria.vadilloh@juntaex.es (J.M.V.); henar.prieto@juntaex.es (H.P.)

Abstract: Groundwater pollution in intensive horticultural areas is becoming an increasingly important problem. Over-fertilization of these crops, combined with poor irrigation management, leads to groundwater contamination through leaching. Previous research on the effect of N on sweet peppers grown in greenhouses is abundant, but data on outdoor cultivation, especially considering variety and site influences, are lacking. Therefore, this study evaluates nitrogen (N) fertilization in open-field processing-pepper crop in Extremadura, Spain to mitigate this environmental impact. Field trials were conducted in 2020, 2021, and 2022 to determine the optimum N fertilizer rate for processing peppers, with the aim of reducing environmental impacts such as nitrate leaching while maintaining crop yields. The trial consisted of applying different N doses, 0, 60, 120, and 180 kg N/ha in 2020 and 2021 and 0, 100, and 300 kg N/ha in 2022. There were four replications of each treatment, arranged in randomized blocks. Measurements included crop yield, biomass, intercepted photosynthetically active radiation (PAR), and canopy cover. The study also developed a critical nitrogen curve (CNC) to determine the minimum N concentration required for optimal growth. The commercial yield results showed that there were no significant differences between the two treatments with higher N inputs in the three years; therefore, the application of more than 120 kg N/ha did not significantly increase yield. Nitrogen-free treatments resulted in earlier fruit maturity, concentrating the harvest and reducing waste. In addition, excessive N application led to environmental problems such as groundwater contamination due to nitrate leaching. The study concludes that outdoor pepper crops in this region can achieve optimal yields with lower N rates (around 120 kg N/ha) compared to current practices, taking into account that initial soil N values were higher than 100 kg N/ha, thereby reducing environmental risks and fertilizer costs. It also established relationships between biomass, canopy cover, and N uptake to improve fertilization strategies. These data support future crop modeling and sustainable fertilization practices.

Keywords: horticulture; open field; vegetative development; nitrogen; CNC; processing pepper

Citation: Vadillo, J.M.; Campillo, C.; González, V.; Prieto, H. Assessing Nitrogen Fertilization in Processing Pepper: Critical Nitrogen Curve, Yield Response, and Crop Development. *Horticulturae* **2024**, *10*, 1141. https://doi.org/10.3390/horticulturae10111141

Academic Editor: Luca Incrocci

Received: 18 September 2024
Revised: 22 October 2024
Accepted: 24 October 2024
Published: 25 October 2024

1. Introduction

The crop area for outdoor sweet pepper in Spain as a whole is only around 28% of the same crop grown in greenhouses, although in some areas (Extremadura, Castilla La Mancha, Navarra) the outdoor version equates to 99% of the total surface [1] and is acquiring increasing importance.

Several studies have been conducted on the effect of nitrogen (N) fertilization on greenhouse-cultivated sweet bell pepper [2–7]. Little, however, has been published on the response to N fertilization of outdoor sweet-pepper cultivation, and more information needs to be generated on the important influence of varieties and locations on the agronomic response of the crop. Saqib et al. (2023) [8] demonstrated the difference shown by different cultivars at different N doses in outdoor peppers under semi-arid conditions. A study with environmental conditions similar to those of the Extremadura region was carried out by

Sambo et al. (2004) [9], but with an old cultivar (cv. Tolomeo) that was exposed to different N doses to analyze canopy reflectance and relate it to different N levels.

A decisive role is played by N in maximizing crop production [10] due to its importance in photosynthesis-driven energy formation and plant growth [11,12]. Therefore, a common practice in intensive horticultural production to ensure the highest yields is overfertilization, a practice that has been associated to nitrate leaching losses that result in groundwater contamination [13,14]. The excessive use of N fertilizers also increases soil N_2O emissions, altering the global N balance over the last few decades [15,16]. In addition to these important problems, the consumption of raw products with high nitrate content poses a risk for human health [17,18]. Excessive fertilization rates, low efficiency of crop N absorption [13,19], and excessive irrigation [20,21] are common practices in horticultural cropping systems. In Spain, some areas of horticultural production have been declared 'Vulnerable zones to pollution caused by nitrates from agricultural sources' [22]. Despite a compulsory action program that limits the amount of irrigation water, N fertilizer, and manure that can be used, this directive has not been as strictly applied in southern European countries as it has in northern European ones such as Belgium, Germany, the Netherlands, or Denmark. Greater pressure from the EU to further reduce the nitrate pollution of surface and ground waters can be expected in the coming years. In addition to the increasing legislative pressure to reduce N losses to water bodies, vegetable growers are also subject to pressure from consumers who increasingly wish to purchase vegetable produce from non-contaminating production systems [23].

The key to reducing the groundwater pollution caused by nitrate leaching or runoff is to clearly define the crop irrigation and N requirements [24,25]. For some vegetable crops, this information is scarce, and more research is needed to ensure safe and sustainable production [26]. In summary, there is an urgent need to contrast efficient methods of irrigation and N management that are successful in open-field vegetables in terms of reducing water and N losses and thereby minimizing surface and groundwater pollution, whilst at the same time maintaining crop yield. In addition, adjusting the dose to the specific requirements of the crop constitutes an economic benefit for growers. The cost of N fertilizer has increased significantly in recent years, with a 300% price surge observed in 2021 [27]. This has highlighted the need for efficient and accurate management strategies to optimize the use of current N fertilizers. Such strategies require a dynamic understanding of crop N demand and supply [16].

The design of an N fertilizer program is closely correlated to the plant's nutrient absorption along the crop cycle. The process is complex, and the factors influencing nutrient availability to the plant and uptake are many and varied. These include weather conditions, the physical and chemical characteristics of the soil, and the influence of agronomic practices. Therefore, models try to integrate all these variables and simulate them to ensure that the plant has the necessary mineral elements at its disposal throughout the crop cycle. These models are interesting for research, academic purposes, or for supporting farmers and technicians, depending on their complexity. Currently, a few tools are available for efficient fertilization management of vegetable crops, including EU-Rotate_N [28], Azofert [29], N-Expert 4 [30], and the VegSyst model [31]. In order to support farmers more directly in optimizing fertilization patterns, the VegSyst DSS (Decision Support System) was developed based on the VegSyst model [32], initially for greenhouse horticultural crops [31,33–35], and later adapted to outdoor crops [36]. As a lot of crop data are needed for the development of these models, the continuous generation of relevant information is important.

A further beneficial addition to fertilizer recommendation systems is the incorporation of nutritional status indicators, which enable the verification of whether the objectives of the fertilization plan are being met. One proposed methodology to identify when a crop is in deficiency is the critical nitrogen curve (CNC). Specific CNCs have been determined for several crop species such as wheat [37,38], rice [39,40], maize [41,42], potato [43,44], processing tomato [45], greenhouse tomato [46], and cucumber [47]. The nitrogen nutritional

index (NNI) is derived from the CNC by relating the critical N content of the curve to the actual N content, which would indicate nutrient excesses and deficits.

The objectives of this study are (i) to analyze the agronomic response (yield) of processing peppers under different N fertilization rates in the Extremadura environment; (ii) to obtain useful information to optimize the fertilization of outdoor pepper; and (iii) to generate useful information (CNC, relationship between canopy cover and photosynthetically active radiation (PAR), extinction coefficient) to support future crop-simulation models, based on the requirements of the VegSyst model.

2. Materials and Methods

2.1. Experimental Setup

Three field experiments (2020, 2021, and 2022) were carried out in the experimental farm of Finca La Orden (CICYTEX, Badajoz, Spain, 38°51′24.10″ N, 6°40′2.5″ W, datum WGS84), which is similar to those of the intensive horticultural industry of the area. The sweet green pepper plants (*Capsicum annuum* L., cv. Ramonete Lamuyo) were transplanted in the three years by the middle of May in paired rows. There were 16 plots, from 4 treatments and 4 replicates, in 2020 and 2021, and 12 plots, from 3 treatments and 4 replicates, in 2022. Each single plot was 12 × 6 m and included 6 beds with two plant rows and a plant density of 33,000 plants/ha. Of these 6 beds, the 4 central beds were used for all measurements to avoid the edge effect. The treatments were N0 (without N fertilizer), N1 (60 kg N/ha), N2 (120 kg N/ha), and N3 (180 kg N/ha) for the 2020 and 2021 seasons and N0 (without N fertilizer), N1 (200 kg N/ha), and N2 (300 kg N/ha) for 2022. Other macronutrients were applied at the same rate in all N treatments, comprising 100 kg P_2O_5/ha, 150 kg K_2O/ha, and 35 kg CaO/ha in the three years.

A fertigation system was used, placing the irrigation line in the middle of the paired rows. Fertilizations were performed weekly. The distance between two consecutive lines was 1.5 m, with 0.3 m between emitters within the line. The emitters had a discharge flow rate of 1.1 L h^{-1}. Irrigation scheduling was carried out by covering the crop water requirements calculated using the reference evapotranspiration (ETo) and the crop coefficient (Kc). Daily ETo and meteorological data were obtained from the nearest meteorological station of the irrigation advisory network of Extremadura (REDAREX) from a station located on the farm itself. The Kc used was from FAO56. The final water input over the 3 years was approximately 5500 m^3/ha.

The soil was an Alfisol [48], with a loamy texture (19.4% clay, 40.4% sand), pH of 7, low organic matter content (0.62%), high bulk density (1.41 g/cm^3), and low cation exchange capacity (9.41 meq/100 g). The climate is Mediterranean, with a dry season from June to September. The average annual precipitation is 500 mm, 80% of which is concentrated from October to May.

2.2. Crop Measurements

2.2.1. Intercepted Photosynthetically Active Radiation (PAR)

The fraction of photosynthetically active radiation intercepted by the crop (fi-PAR) was determined at solar noon [49,50] by measuring PAR above (PAR_a) and below (PAR_b) the canopy. PAR_b was measured by placing two ceptometers (Accupar LP-80) perpendicularly to the drip irrigation line, one at each side, covering the width of two crop lines. One measurement was the average of 10 readings, taken by moving the ceptometers every 10 cm along the line. At the same time, the PAR above the canopy (PAR_a) was recorded.

fi-PAR was then calculated as:

$$\text{fi-PAR} = \frac{PAR_a - PAR_b}{PAR_a} \quad (1)$$

The measurement was carried out on several days throughout the growing cycle, selecting different stages of canopy ground cover at each session.

2.2.2. Fraction of Crop Ground Cover

The fraction of crop cover (f_{CC}) was measured at midday with a commercial digital camera (Nikon Coolpix A300, Nikon, Tokyo, Japan). Photographs were taken at solar noon to enhance the distinction between soil and crop pixels and by positioning the camera at a height of 215 cm above the soil. Each photograph encompassed the entire width (150 cm) and length (80 cm) of the bed. On each sampling day, measurements were taken at the same times and locations as the PAR measurements. The images were classified according to the radiation levels displayed in an RGB crop image (0 to 255 colors) using the maximum reclassifying tool of the GIMP 2.8. software. The images were processed in accordance with the 'reclassification method' described by Campillo et al. (2008) [51]. Figure 1 shows an example of the zenithal images used to calculate the f_{CC} via RGB reclassification.

Figure 1. Zenithal photo of the crop performance 'reclassification method'.

To obtain the seasonal course of the f_{CC}, photographs were always taken in the same preselected area (3 × 3 m) of each elemental plot at weekly intervals until maximum ground cover.

2.2.3. Crop Dry Matter (DM) and Leaf Area Index (LAI)

Measurement of seasonal aerial crop dry matter (DM) was carried out after sampling 4 plants/plot every 2 weeks throughout the crop cycle. There were 10 sampling dates in 2020, 7 in 2021, and 10 in 2022. Plants were split into leaves, flowers, stems, and fruits; weighed separately; and then dried in a dryer at 65 °C to constant weight. Total dry weight was calculated as the sum of the weight of the four organs and then referred to kg/ha considering the planting density [6].

In 2020, 2 plants per single plot were separated from the biomass sample, and the leaves were separated from the rest of the plant. The leaf area was measured using a planimeter (Li 3000, LiCor, Inc., Lincoln, NE, USA). The leaves were dried and weighed to obtain the ratio of leaf area to leaf dry weight, which was applied to all leaves in the biomass sample. The leaf area index (LAI) was then calculated as the total leaf area divided by the sample area.

2.2.4. Extinction Coefficient

The relationship between fi-PAR and the LAI can be written as:

$$f_{i\text{-}PAR} = 1 - e^{-k*LAI} \quad (2)$$

where k is the extinction coefficient for PAR radiation. From this equation, k can be written as:

$$k = -\frac{Ln(1 - f_{i\text{-}PAR})}{LAI} \quad (3)$$

(Kiniry et al., 2011; Lacasa et al., 2021; Monsi et al., 2005) [52–54]

LAI measurements were made with an LI-3100C area meter (Li-Cor, Inc., Lincoln, NE, USA). These measurements were taken by swiping the leaves of the plants sampled by the LI-3100C in the DM productivity samplings in the 2021 season.

2.2.5. Crop Nitrogen Uptake

The amount of nitrogen taken up by each organ (kg N/ha) was calculated for each biomass sampling as the product of its dry matter (kg/ha) and its N content. The N content was measured in dried samples with a Eurovector EA3000 elemental analyzer (Eurovector Srl, Pavia, Italy).

2.2.6. Critical Nitrogen Curve (CNC)

The CNC represents, for a given total crop dry matter, the minimum crop N concentration for the full plant that produces the highest dry matter. In this study, it was calculated following the methodology of Greenwood et al. (1990) [55] and Padilla et al. (2016) [56]. For each sampling date, the N treatment showing the highest DM production was determined by running an analysis of variance (ANOVA), and these values, together with their N content, were used to calculate the CNC. For those sampling dates when more than one N treatment showed the highest DM production, the one with the lowest N content was selected. Based on these data, we fitted a negative power relationship:

$$N_{crit} = a \times TDM^{-b} \quad (4)$$

where N_{crit} is the critical N concentration (%), a is the N concentration when DM production is 1 t ha^{-1} [37,57], and b is the decline of N content as DM production increases. Note that N contents of DM lower than 1 t ha^{-1} were not considered as the dilution of crop N in young plants is not clear [37,55].

2.2.7. Crop Yield

Harvests dates were 25 August, 99 days after transplant (dat); 2 September (107 dat) and 30 September (135 dat) in 2020; and 30 July (77 dat), 31 August (109 dat), and 15 September (124 dat) in 2021. In the 2022 season, the first harvest was on 2 August (82 dat), and the last was on 23 August (103 dat) for N0 and on 6 September (117 dat) for N1 and N2. To quantify crop yield, we sampled three linear meters of the plants in the central area of each elemental plot. On each harvest date, commercial green and red fruits and non-commercial fruits, depending on the size, were weighed separately. Total commercial yield (t ha^{-1}) was obtained by adding the fresh weight of commercial green and red fruits of all the harvest dates.

2.2.8. Soil Sampling for Mineral Nitrogen Determination

N content in soil was sampled just before transplanting and at the end of the crop cycle after harvesting. Sampling points within each plot were taken approximately 20 cm from the drip line, between each plant. The 4 points were distributed in each plot to cover almost the entire surface, taking two samples at each point, from 0–20 cm and 20–40 cm depth. After drying and sieving the soil samples, the nitrate and ammonium content was analyzed with an Evolution 201/220/260 UV–Visible spectrophotometer (Thermo Fisher Scientific, Waltham, MA, USA). Nitrate content was measured according to the methodology of Sempere et al. (1993) [58], and ammonium was measured following Rhine et al. (1998) [59]. The initial N situation for the field trials was 177 kg N/ha on average in 2020, 149 for 2021, and 92 for 2022.

2.3. Data Analysis

The seasonal evolution of the different variables is presented in terms of cumulative growing degree days (GDDs) calculated through the formula:

$$GDD = \sum \frac{Tmax - Tmin}{2} - Tbase \quad (5)$$

where Tmax is the maximum temperature of the day, Tmin the minimum temperature of the day, and Tbase is the minimum temperature at which the crop grows, which for the pepper crop is considered to be 10 °C [60].

The experimental data of the three years were evaluated through ANOVA after verifying the normality and equality of variance. Significant differences were determined at $p \leq 0.05$, using Tukey's test to compare the DM content, yield, and fi-PAR. The SPSS 22 (IBM Corp., Armonk, NY, USA) was used for all the statistical analyses. Microsoft 365 Excel software was used to determine the equations correlating different variables and their coefficient of determination (R^2).

3. Results

3.1. Crop Evolution Under No Limiting Nitrogen Conditions

3.1.1. Growing Conditions

Over the three years of the trial, the average monthly maximum temperature ranged from 34.1 to 44.4 °C, and the average minimum ranged from 8.7 to 22 °C. As shown in Table 1, the warmest months were July in 2020 and 2022 and August in 2021. The warmest year was 2022, with an average maximum temperature of 44.4 °C in July. In all years, there was a very low level of rainfall during the growing season.

Table 1. Climate data for 2020, 2021, and 2022 based on each season's crop cycle.

Months	Tª Maximum (°C)			Tª Minimum (°C)			R. Humidity (%)			Precipitation (mm)		
	2020	2021	2022	2020	2021	2022	2020	2021	2022	2020	2021	2022
May	34.6	34.1	37.6	10.1	8.7	9.9	58.3	55.8	52.6	0	0	0
June	38.6	36.1	41	9.6	8.7	10.7	56.9	56.9	52.5	0	28.5	0
July	41.1	40.3	44.4	12.4	11.6	14.1	47.7	52.8	43.8	10.3	0	0
August	39.2	42.8	40.7	11.9	12	22	52	51.5	49.3	0	1	0
September	36.7	37.9	31.7	12.5	14.9	14.4	44.7	60.7	55.4	0	51.5	0

Figure 2 shows the reference evapotranspiration data in millimeters per day. Fluctuations between 4 and 8 mm are observed due to weather variations, with evapotranspiration peaking on certain days and dropping toward the end of the period. These data were used for daily irrigation scheduling.

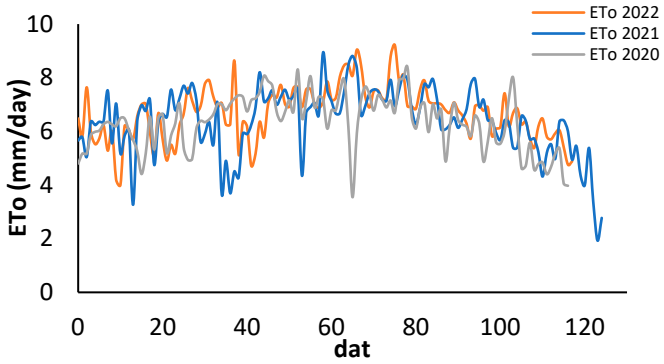

Figure 2. Daily ETo evolution of the 2020, 2021, and 2022 campaigns.

3.1.2. Analysis of Crop Growth and Development

After transplanting, there was a period of plant establishment with little growth, which lasted until 400 cumulative GDDs in 2020 and 2021 and 600 GDDs in 2022 (Figure 3). From this point onwards, the increase in above-ground parts dry-matter accumulation was linear with cumulative GDDs until harvest. In all three years, the linear fit was significant, with an R^2 greater than 0.94. However, the equations were different, with slopes ranging from 4.93 in 2022 to 9.93 in 2020.

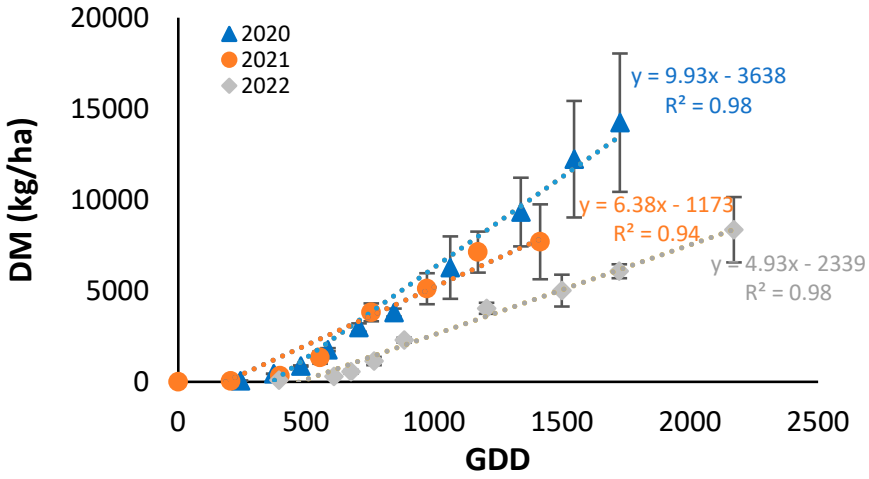

Figure 3. Seasonal evolution of cumulative dry matter (DM) as a function of growing degree days (GDDs) under non-nitrogen limiting conditions for the years 2020, 2021, and 2022, (N3 for 2020 and 2021 and N2 for 2022). Each point is the average of 4 measurements in the elementary replicate plots.

The relationship between the f_{CC} and fi-PAR (Figure 4) was linear and coincident in both years with a very good fit (R^2 = 0.99) and very close to the 1:1 line. fi-PAR values were slightly lower than f_{CC} ones.

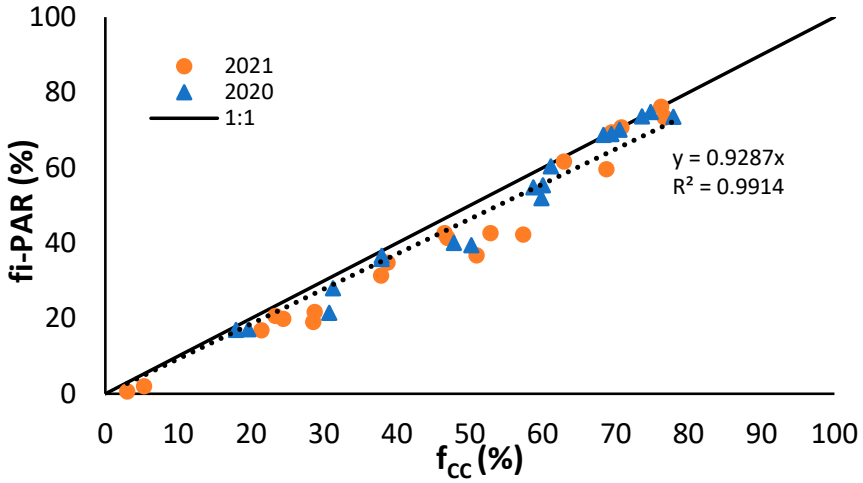

Figure 4. Relationship between the percentage of crop cover (f_{CC}) and fraction of photosynthetically active radiation (PAR) intercepted by the vegetation cover (fi-PAR) obtained in the years 2020 and 2021. Each point corresponds to the measurements made on the same section of crop.

As illustrated in Figure 5, the seasonal evolution of the fi-PAR was fitted to a logarithmic equation following the post-transplanting shutdown period. The trend was similar in each season, except in the period from GDD 900 to GDD 1200 when the data from the 2022 season were below the trend line.

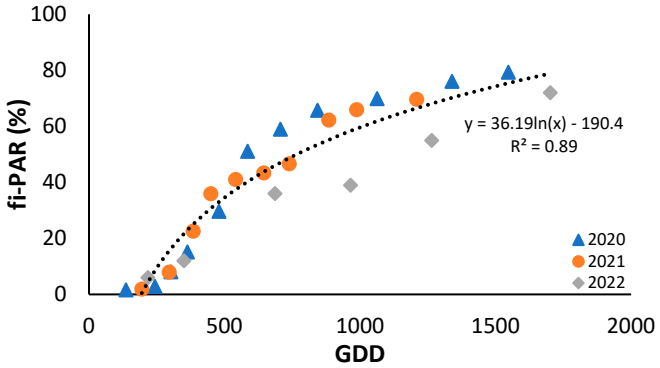

Figure 5. Evolution of fi-PAR along the crop cycle expressed in cumulative growing degree days (GDDs) for 2020, 2021, and 2022 under non-nitrogen limiting conditions (N3 for 2020 and 2021 and N2 for 2022).

The relationship between above-ground parts dry-matter accumulation and the fi-PAR (Figure 6) was also logarithmic, with the three years fitting the same equation.

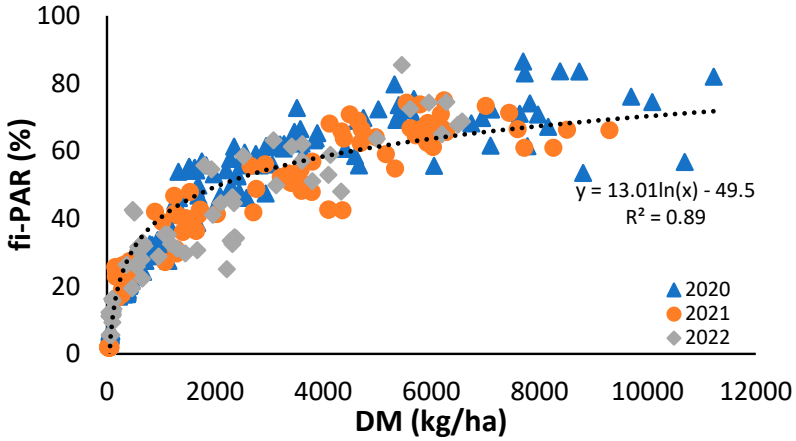

Figure 6. Relationship between cumulative dry matter (DM) along the crop cycle and the fraction of photosynthetically active radiation (PAR) intercepted by the crop (fi-PAR) for the years 2020, 2021, and 2022. Each point is the average of 4 measurements in the elementary replicate plots.

The extinction coefficient calculated with the data from 2021 by Equation (3) was $k = 0.48$, with an $R^2 = 0.75$ between LAI and Ln(1 − fi-PAR).

3.1.3. Critical Nitrogen Curve (CNC)

Figure 7 shows the CNC developed in this work using the data obtained in the field experiments of the three years. The CNC published by Rodríguez et al. (2020) [6] for sweet pepper grown in a greenhouse and the CNC published by Lemaire and Gastal (1997) [61] for C3 plants are also shown. Although following a similar pattern, the curve developed for open-field sweet pepper is much lower than that for pepper in a greenhouse, and it is closer but also slightly lower than the curve published by Lemaire. As in other crops, N_{crit} decreases as DM increases. The equation obtained was $N_{crit} = 3.86 * DM^{-0.29}$ ($R^2 = 0.86$) (Equation (4)), where N_{crit} is the critical crop N content, 3.86 is the total crop N content (%) for DM production of 1 t ha^{-1}, and −0.29 is the value of a dimensionless parameter that describes the slope of the relationship with which N content declines with increasing DM, the dilution coefficient.

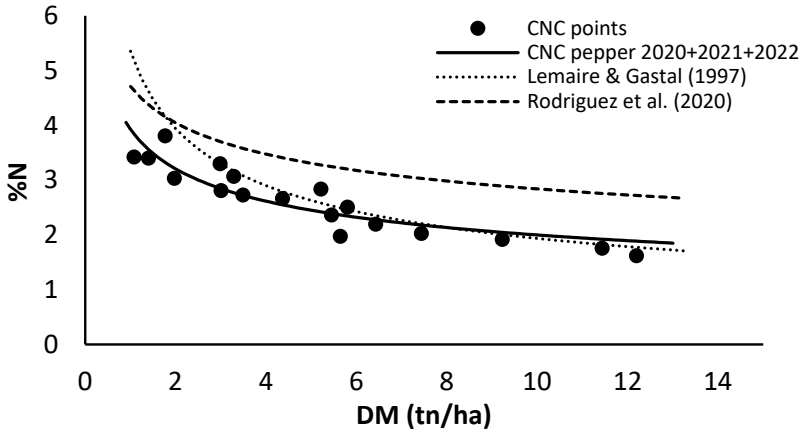

Figure 7. Critical N curve (CNC) for sweet pepper grown in open fields using total crop N content and total DM (continuous black line), CNC for C3 crops of Lemaire and Gastal (1997) [61] (dotted line), and CNC for greenhouse sweet pepper of Rodríguez et al. (2020) [6] (dashed line).

3.2. Response of Pepper Crop to Different Doses of Nitrogen (N) Fertilization

3.2.1. Vegetative Development and Flowering

Figure 8 shows the evolution of fi-PAR for the different N treatments in the three years. The seasonal pattern of fi-PAR in 2020 and 2021 was identical: after the post-transplant period, there was a rapid increase in crop cover between GDD 400 and GDD 600, followed by a slowdown. In 2022, the increase in fi-PAR was progressive throughout the cycle, unlike in the previous two years. In 2020, the maximum fi-PAR was 80% in the N2 and N3 treatment, a value higher than those seen in the following two years.

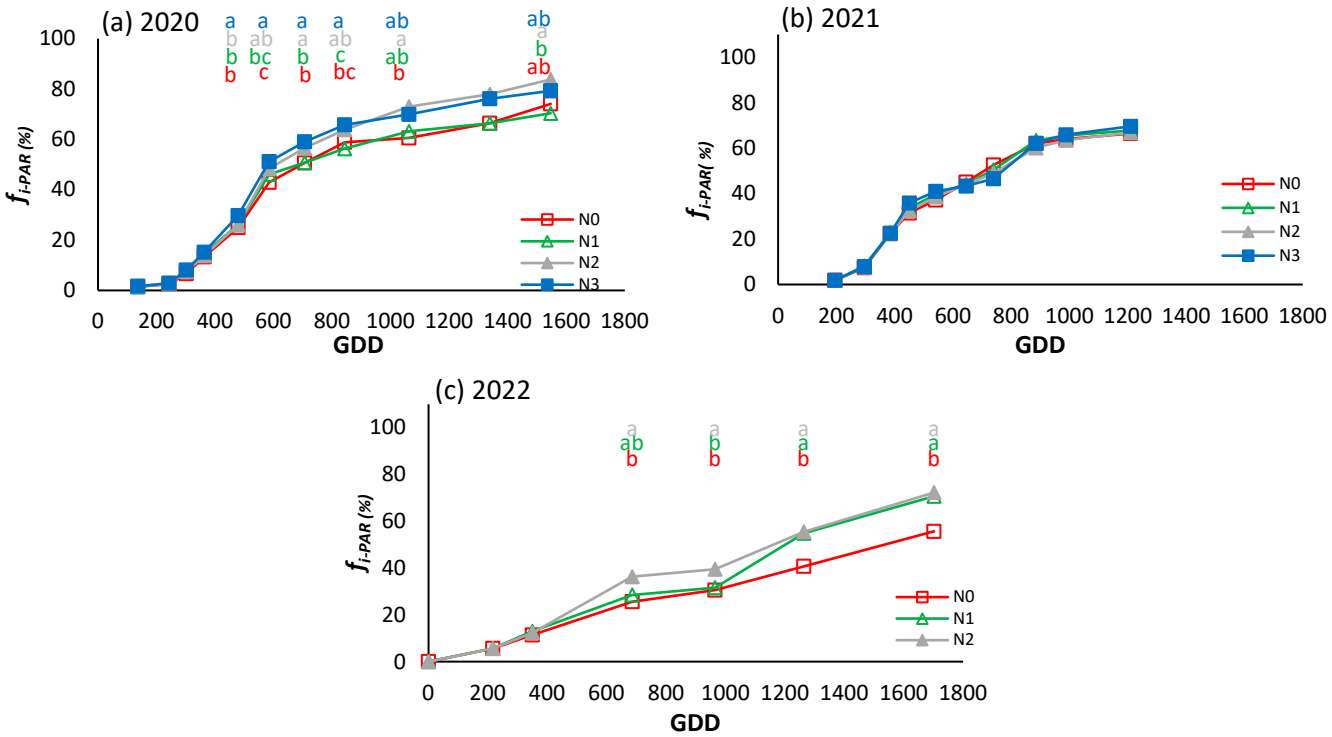

Figure 8. Evolution of the fraction of PAR intercepted by the crop (fi-PAR) for the different N treatments in 2020 (**a**), 2021 (**b**), and 2022 (**c**). Each point is the average of 4 measurements in the elementary replicate plots in each treatment. Letters indicate whether there are significant differences between treatments in each sample for $p \leq 0.05$. In samples where no letters appear, there were no significant differences between treatments.

Canopy development differed between treatments in 2020 and 2022. In 2020 (Figure 8a), there were significant differences from GDD 478. From this point onward, the treatments were grouped in pairs, differentiating between the most and least fertilized and equalized at the end of the cycle. In 2022, the canopy in the N0 treatment was less developed than in the other two treatments, with maximum differences in the last sampling.

Figure 9 illustrates the seasonal evolution of the dry weight of flowers over the first two years. In both years, the pattern was similar, with the appearance of the first flowers occurring at approximately 200 GDDs, followed by a rapid increase to a maximum at 585 GDDs in 2020 and 554 GDDs in 2021, followed by a subsequent decrease. In 2020, there was a rebound to 1726 GDDs, while in 2021 a certain flowering rate was maintained, with a higher rate observed in N0 than in the other treatments. In order to comprehend the discrepancies observed in the final stages, it is essential to consider the extended growing season that was experienced in 2020.

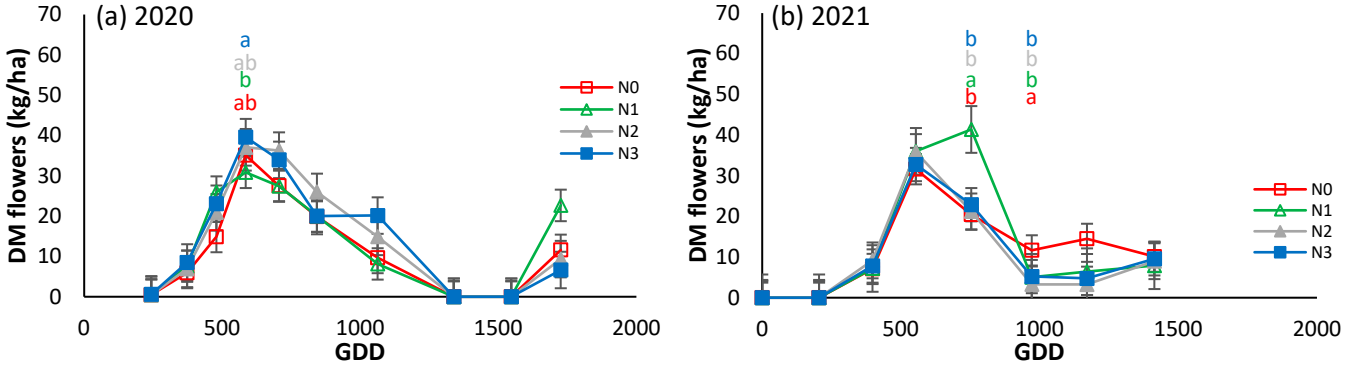

Figure 9. Evolution of flower production expressed in dry matter (DM) for the different N treatments in the (**a**) 2020 and (**b**) 2021 seasons. Each point is the average of 4 measurements in the elementary replicate plots in each treatment. Letters indicate whether there are significant differences between treatments in each sample with $p \leq 0.05$. In samples where no letters appear, there were no significant differences between treatments for $p \leq 0.05$.

The production of dry matter in 2020 was markedly higher than in the subsequent two seasons (14.2 tn/ha for N3) (Figure 9). The statistical differences in total dry matter between treatments are in accordance with those obtained in the evolution of the fi-PAR, with N0 exhibiting lower values than N3 throughout the crop cycle. N1 and N2, in contrast, demonstrated intermediate values, with significant differences between them observed in certain sampling periods. In 2021, no significant differences were observed between the treatments, with dry matter yields at the end of the crop cycle reaching 6.4–7.7 tn/ha. In 2022, a clear distinction was evident between N0 and the other two treatments, with notable disparities emerging from the fourth sampling onwards. Conversely, treatments N1 and N2 exhibited no discernible differences between them. The highest biomass production in 2022 was 8.35 tn/ha in N2, while N0 exhibited the lowest aerial-parts dry matter at the conclusion of the three-year trial, with a final yield of 4.5 tn/ha. The N0 treatment exhibited a shorter growing season, resulting in the last DM sampling being conducted at an earlier point in time relative to N1 and N2. For the purposes of statistical analysis, the last samplings of the three treatments were grouped together, despite the fact that the samples were taken on different days.

As can be seen in Figure 10, most of the biomass corresponds to the fruits, so that after the flowering peak at GDD 585 (Figure 8), from GDD 600 onwards, fruit set and subsequent fruit growth are mainly responsible for the increase in biomass.

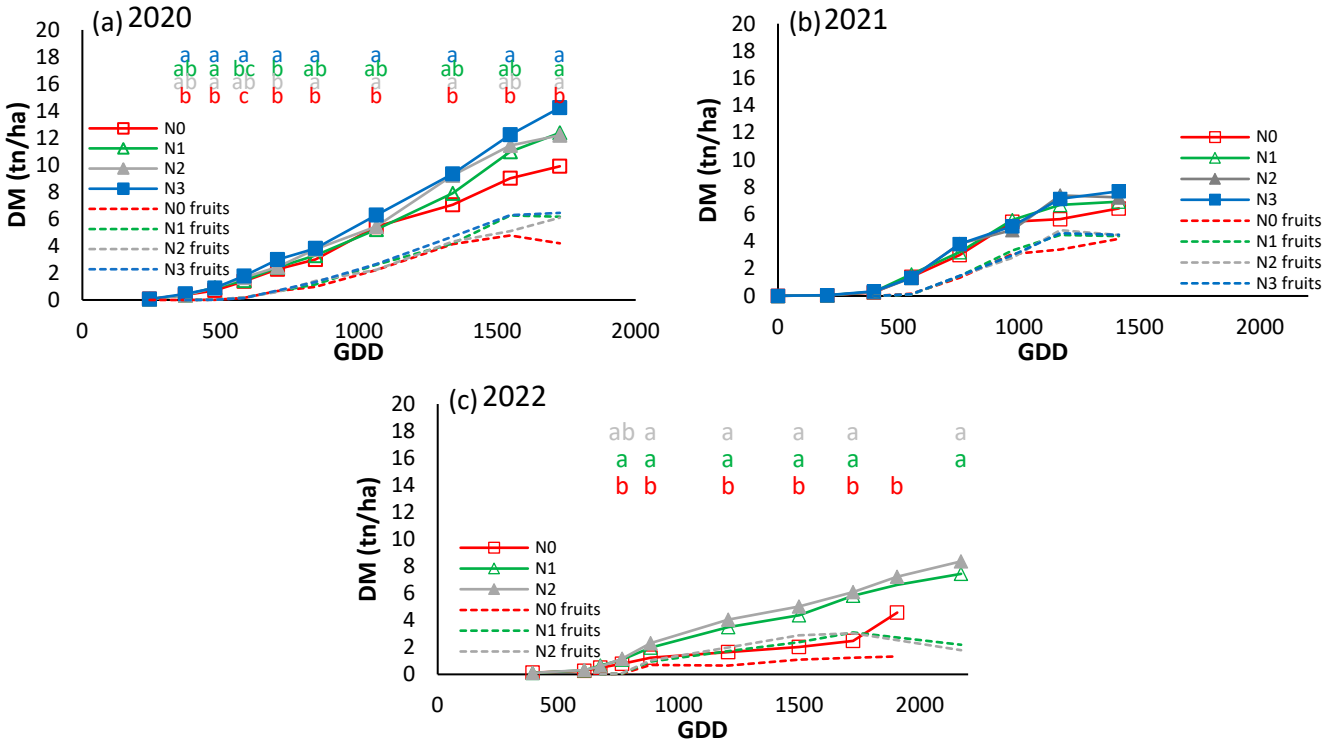

Figure 10. Total dry matter and fruit dry matter evolution in cumulative growing degree days (GDDs) for the different treatments in (**a**) 2020, (**b**) 2021, and (**c**) 2022. Each point is the average of 4 measurements in the elementary replicate plots in each treatment. Letters indicate whether there are significant differences in total dry matter between treatments in each sample with $p \leq 0.05$.

3.2.2. Crop Yield

Figure 11 shows the fresh weight of commercial fruit in successive harvests. The year 2020 was the most productive regarding total fruit of four harvests. There were three harvests in 2021 and two in 2022, with the latter year being the least productive (Table 2). In both 2020 and 2021, the differences in fruit production between treatments were minimal, with the least productive treatments being N1 in 2020 and N0 in 2021. In 2020, N0 demonstrated an advancement in production, exhibiting higher fruit weights in the initial and subsequent harvests. Conversely, both N0 and N1 exhibited a decline in fruit production in comparison to the other two treatments in the subsequent two harvests. In 2021, no difference existed between treatments in the fruit weights of each of the harvests, although N0 was below the others regarding the cumulative weight.

As shown in Figure 9, the highest flowering intensity is grouped from 30 dat onwards. There was also a higher initial soil availability of N (nitrate and ammonium) at the beginning of the cycle in 2020 (177 kg N/ha) compared to 2021 (149 kg N/ha) as it was partly absorbed by the crop since the final nitrogen was 44 kg N/ha in 2020 and 43 kg N/ha in 2021. As for the difference in fruit production between treatments, in 2020 there were only significant differences in N2, which was higher than the rest of the treatments. However, in 2021 N0 was significantly lower than N1, with no differences between the rest of the treatments.

The grouping of peppers destined for industry is an important aspect of reducing costs through mechanization. The reduction in N application resulted in a more concentrated and earlier production, with 41% of the total in the first harvest in N0 in 2020 and 57% in 2021. This yielded 10% more than the rest of the treatments in 2020 and 7% more in 2021 (Figure 10). As indicated in Table 2, this also signifies a lower proportion of waste in the N0 treatments across both seasons (13% and 15%).

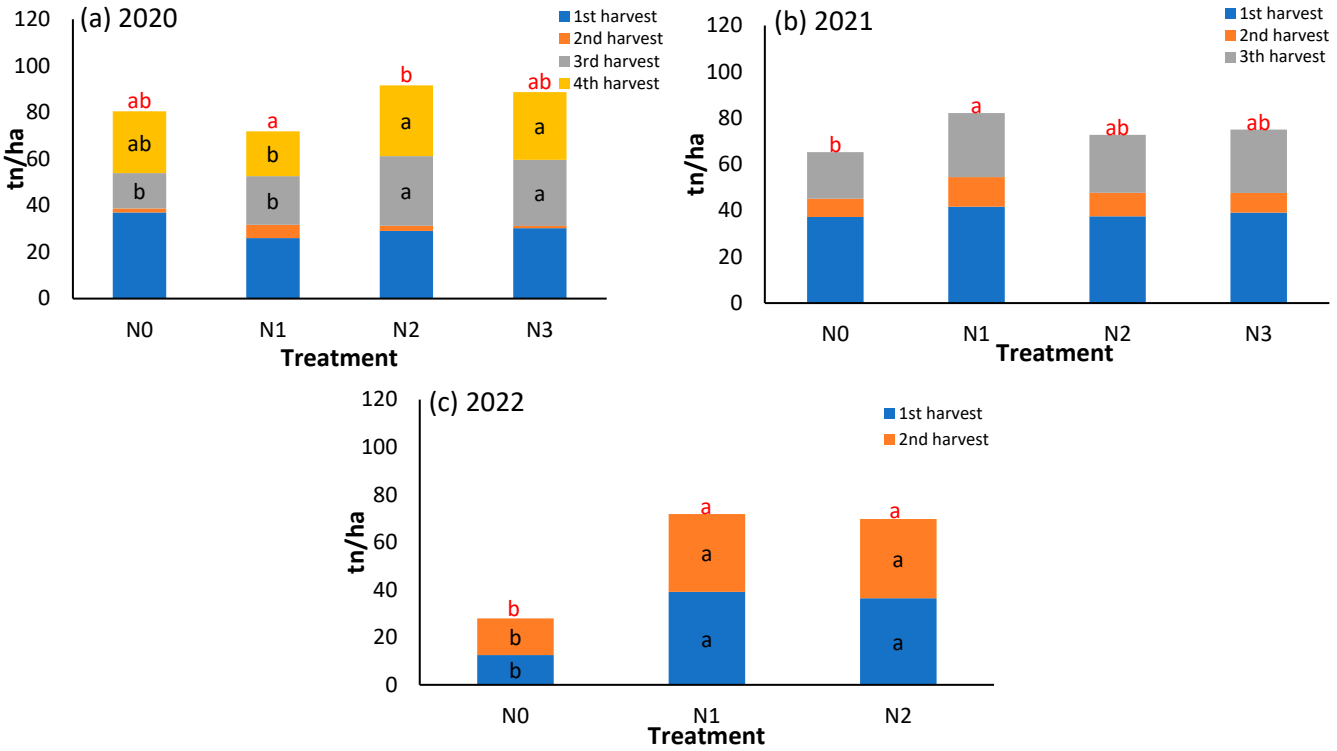

Figure 11. Commercial fruit production of seasons (**a**) 2020, (**b**) 2021, and (**c**) 2022 per harvest for treatments. Black letters indicate whether there are significant differences in each individual harvest, and red letters indicate significant differences in total yield.

Table 2. The yield of fresh fruit produced over the three experimental years classified into commercial and total categories, together with the total number of fruits differentiated by treatments. The share (%) of commercial fruit with respect to the total for each harvest is shown in brackets. Letters indicate whether there are significant differences between treatments in each sampling for $p \leq 0.05$.

	2020			2021			2022		
	Commercial (tn/ha)	**Total (tn/ha)**	**Total n°. Fruit (n°/ha)**	**Commercial (tn/ha)**	**Total (tn/ha)**	**Total n°. Fruit (n°/ha)**	**Commercial (tn/ha)**	**Total (tn/ha)**	**Total n°. Fruit (n°/ha)**
N0	80.4 (87) ^{ab}	92.3 ^{ab}	788,658	65.2 (85) ^{b}	77.2 ^{b}	749,213	25.9 (90) ^{b}	28.9 ^{b}	465,838
N1	71.8 (83) ^{b}	86.8 ^{b}	672,798	82.1 (81) ^{b}	101.9 ^{a}	1,158,193	69.7 (92) ^{a}	75.9 ^{a}	566,067
N2	91.6 (85) ^{a}	107.6 ^{a}	752,440	72.7 (82) ^{b}	88.9 ^{ab}	1,186,093	71.8 (92) ^{a}	77.9 ^{a}	564,159
N3	88.7 (84) ^{ab}	106.2 ^{ab}	798,368	75.0 (80) ^{b}	93.5 ^{ab}	1,154,012			

3.2.3. Nutritional Status and N Uptake

Figure 12 illustrates the seasonal evolution of N concentration in the diverse aerial organs over the two-year period of 2020 and 2022. In both cases, the evolution was characterized by a decrease in N concentration in the three organs from GDD 500 to GDD 600, with higher levels observed in the leaves and lower in the fruits. The year 2020 began with higher N concentrations in the leaves than those in 2022, while the values were similar in both years in the other organs. The greatest differences in N content between treatments were observed in the stems of plants in 2020 and in the leaves in 2022. In 2020, the N0 treatment differed from the fertilized treatments, while in 2022, the three treatments differed from each other. In the year 2021, the treatments exhibited a similar trend to 2020. In all cases, the fruits were not particularly sensitive to the various fertilizer strategies.

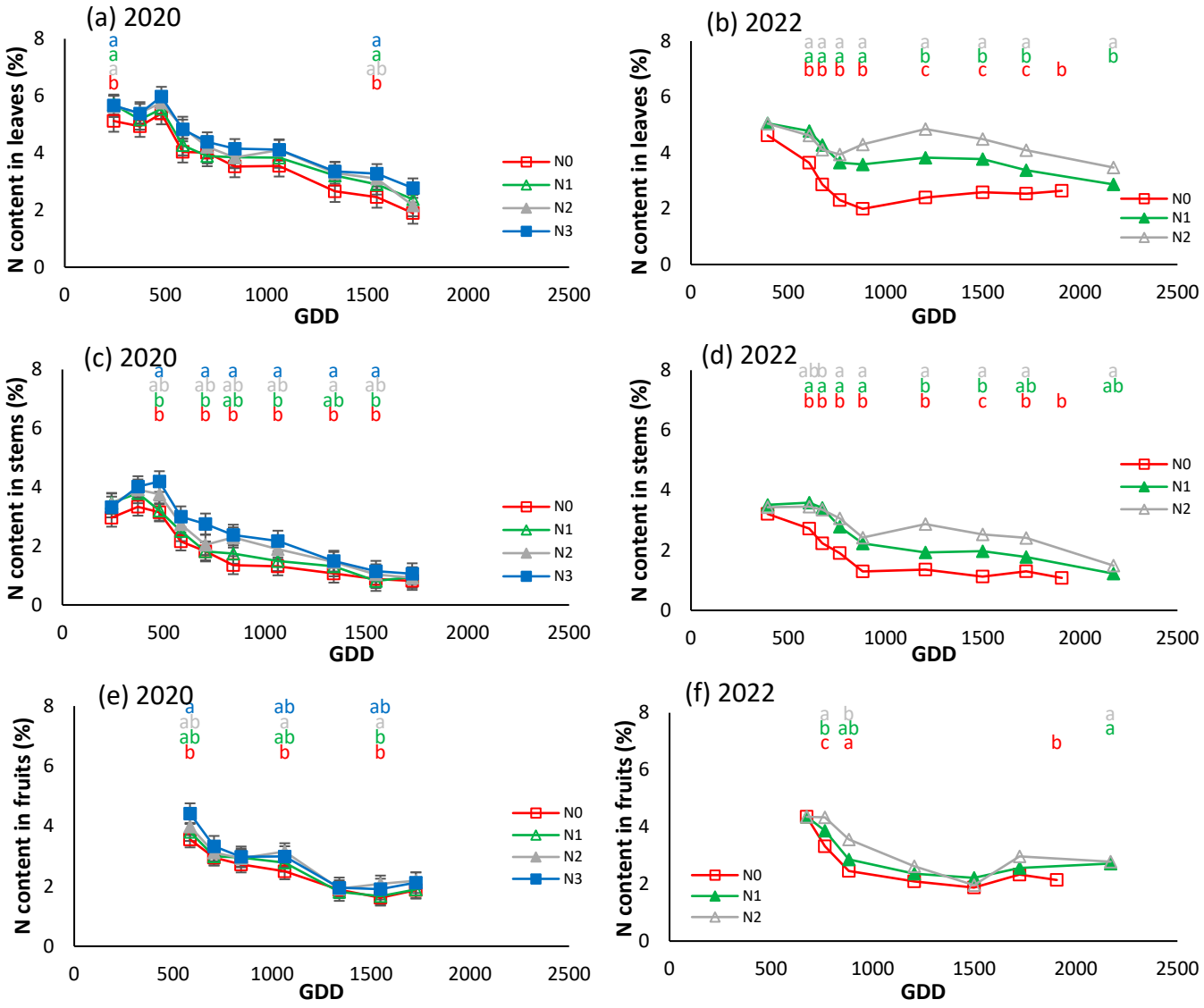

Figure 12. Evolution of the N content in relation to cumulative growing degree days (GDDs) for the different treatments and parts of the plant. (**a**,**b**) correspond to leaves in 2020 and 2022, respectively, (**c**,**d**) to stems in 2020 and 2022, respectively, and (**e**,**f**) to fruits in 2020 and 2022, respectively. Each point is the average of 4 measurements in the elementary replicate plots in each treatment. Letters indicate whether there are significant differences between treatments in each sample with $p \leq 0.05$.

The relationship between N content (%) and biomass produced by the different treatments in the three seasons is shown in Figure 13. Overlaying the developed CNC, in 2020 all treatments follow the curve. In 2021, slight differences are observed between the N2 and N3 treatments compared to N1 and N0 at the beginning and end of the curve, with the largest differences being around 5 tn/ha. For 2022, there is a clear gradual difference in N content between N0, N1, and N2. In this last season, N0 showed an N deficit and consequently a limitation of DM production; N1 was close to the curve while N2 displayed an excessive N percentage showing what Zhang et al. (2008) [62] described as 'luxury' N use. In any case, all treatments follow a clear trend throughout the dry-matter generation process.

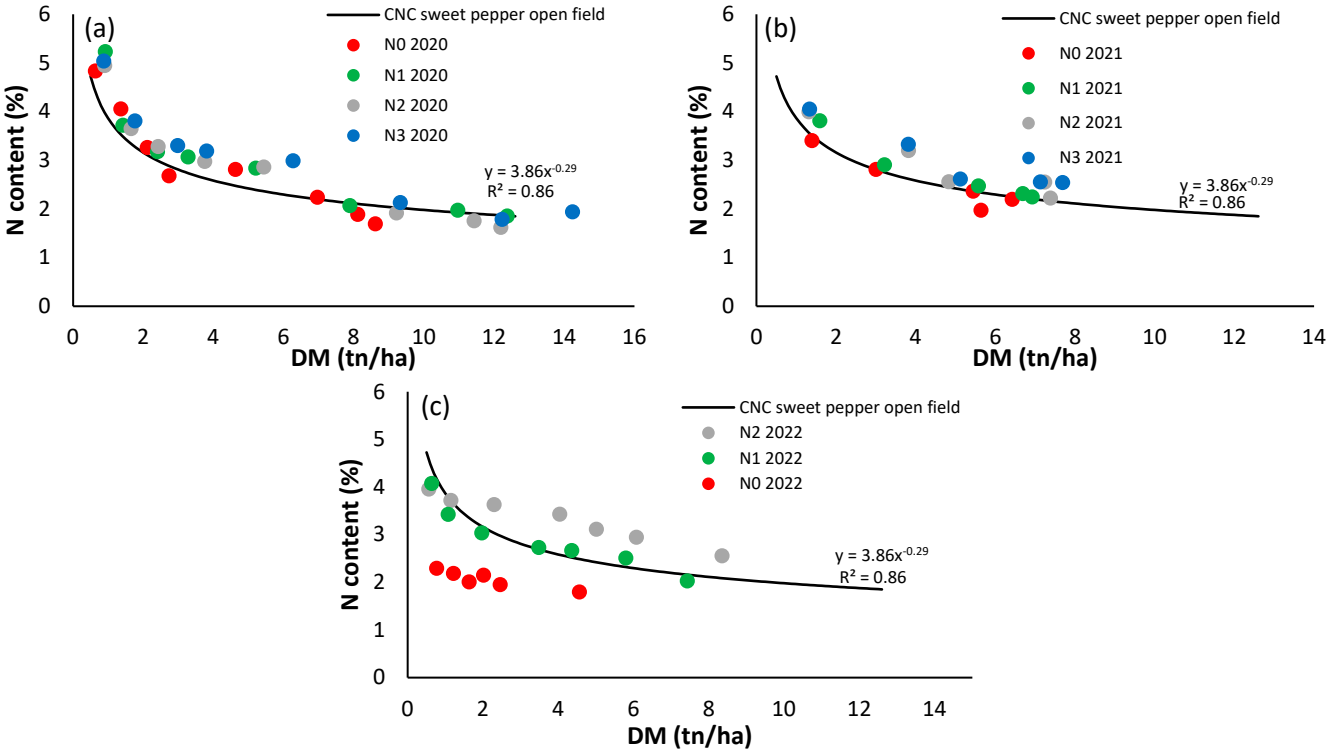

Figure 13. Data on N content (%) in dry matter of aerial parts versus total dry matter (DM) weight over the crop cycle for each treatment in 2020 (**a**), 2021 (**b**), and 2022 (**c**), contrasted with the CNC generated in this work.

3.2.4. Crop N Uptake

Over the three-year period, the seasonal N uptake pattern was closely correlated with above-ground biomass production (Figure 14). The highest uptake was observed in the N3 treatment in 2020, with a total value of 272 kg N/ha. In 2021, the highest uptake was 197 kg N/ha, while in 2022 the value was 224 kg N/ha. At the opposite end of the spectrum, the lowest uptake was observed in the N0 treatment in 2022, with a rate of 89 kg N/ha. In 2020, there were notable discrepancies between the N0 and N3 treatments at various points throughout the cycle, apart from GDD 1063 when no differences were observed between any of the treatments. All treatments exhibit a consistent pattern of uptake throughout the cycle, with progressively higher values observed for N0, N1, N2, and N3, in that order. In the 2021 season, the only differences between N0 and N1 with respect to N2 and N3 were observed at GDD 754 and between N0 and N3 at GDD 1171. The largest differences between treatments were obtained in 2022 (Figure 14c).

As illustrated in Figure 15, fruit production increases with N uptake. However, beyond an N application rate of 200 kg N/ha, the potential for further yield gains is limited under the conditions of this research. This is in response to Mitscherlich's law, which states that yield is a function of fertilization, and that exceeding the optimum dose not only fails to increase yield, but actually reduces it.

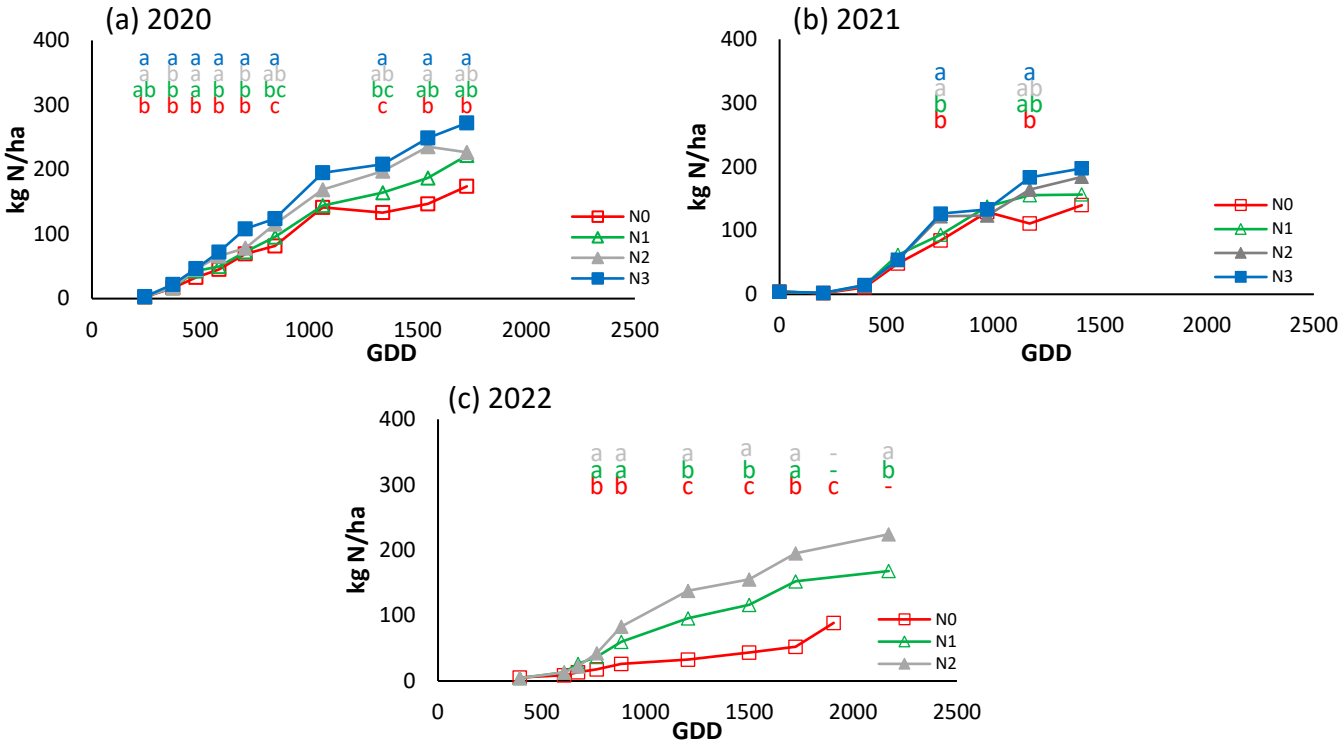

Figure 14. Seasonal evolution of nitrogen (N) uptake in cumulative growing degree days (GDDs) for the different treatments in the years (**a**) 2020, (**b**) 2021, and (**c**) 2022. Each point is the average of 4 measurements in the elementary replicate plots in each treatment. Letters indicate whether there are significant differences between treatments in each sample with $p \leq 0.05$.

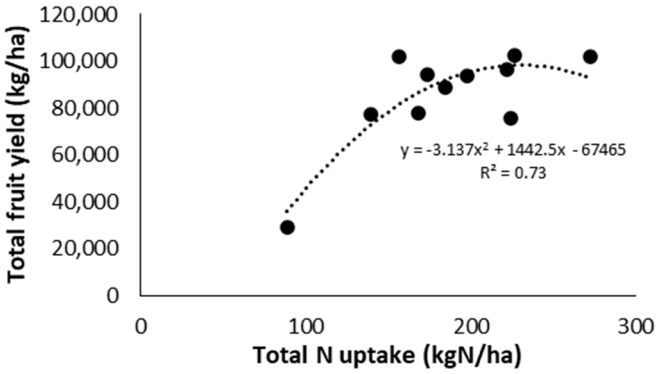

Figure 15. Relationship between total N uptake and total fresh-fruit yield for the years 2020, 2021, and 2022. Each point is the average of 4 measurements in the elementary replicate plots of each treatment.

4. Discussion

The initial section of this paper presents a series of relationships that describe the development pattern of an outdoor industrial sweet-pepper crop, which are of interest for the purposes of crop modeling. Models have been developed for greenhouse pepper, including VegSyst [35] and glasshouse [60], as well as for other pepper varietals, such as chili peppers [63]. However, no models have been developed for processing peppers grown in open fields. Given the changes in management and varietal type, it is necessary to adjust the models to ensure their continued efficacy. In this regard, VegSyst has developed two versions of its model: one for greenhouse tomatoes [32] and another for outdoor processing tomatoes [36]. The information presented here provides a foundation for making the requisite adjustments to ensure the applicability of pepper models to this variety in an open-field setting.

4.1. Interception of Radiation and Crop Growth

The models provide information on crop development under optimal conditions. However, due to the multitude of factors that influence plant development, mainly in open fields, deviations can occur that modify nutrient uptake. A strong correlation has been established between fi-PAR and f_{CC} (R^2 = 0.99), which enables the monitoring of plant canopy development through remote sensing. This, in addition to the relationship between fi-PAR and DM, allows for the real-time estimation of above-ground biomass production. The incorporation of this information into the development models provides a robust estimation of the nutrient uptake pattern, which can be utilized for fertilizer plan corrections.

The relationship between image analysis and the nutritional status of crops is a subject that has been explored in several studies. For example, Mercado-Luna et al. (2010) [64] investigated the relationship between G/(R+G+B) and the N status of tomato crops, while Yuzhu et al. (2011) [65] explored this relationship in pepper crops. The objective of this study is to utilize the images to quantify N uptake along the crop cycle, with a view to making adjustments to fertilization programs. In this regard, Lukia et al. (1999) [66] employed image analysis to estimate the percentage of plant cover and biomass in wheat. However, no such correlation has been identified in the existing literature with regard to pepper. Therefore, we propose that the establishment of such robust relationships between diverse variables, as evidenced in this study, is advantageous for potential modeling in this crop, whether pertaining to irrigation, fertilization, image analysis, or other factors.

4.1.1. Critical N Dilution Curve

The acquisition of a valid CNC for a given crop is of significant interest, not only for the calculation of N uptake based on yield, but also for assessment of the crop's nutritional status. In this study, the curve obtained under the specified experimental conditions was compared with that published by Rodríguez et al. (2020) [6] for greenhouse bell pepper. The two curves exhibit a similar pattern. However, the contents of N in dry matter are consistently lower throughout the cycle in open-field conditions. This discrepancy may be attributed to differences in environmental conditions, management practices, and varietal types. In greenhouses, crops are subject to continuous harvesting, in contrast to outdoor cultivation, which is more spaced. These harvesting practices may promote the continuous production of new photosynthetically active green tissue, thereby maintaining a relatively high N content throughout the greenhouse growing cycle. Another potential reason for this discrepancy is the greater availability of light in greenhouse cultivation, where plants are trellised, resulting in greater height growth and less plant compaction. In contrast, outdoor cultivation is characterized by a rapid reduction in light availability, which subsequently leads to a decline in photosynthesis and a rapid decrease in crop N content [67]. As described by Greenwood et al. (1990) [55], Gastal and Lemaire (2002) [67], Lemaire et al. (2007) [68], and Seginer (2004) [69], planting density has an impact on N dilution, which may have a comparable effect to that discussed above.

By combining the established relationship between fi-PAR, DM, and the CNC, it is possible to derive the following relationship:

$$47.962 \times e^{0.0749 fi\text{-}PAR} = \left(\frac{3.86}{\%N_{crit}}\right)^{1/0.29} \quad (6)$$

This relationship (Equation (6)) allows for the monitoring of the minimum required content of nitrogen content (%) at each phase of the cycle using either drone flights or satellite images. This is made possible by the established correlation between fi-PAR and f_{CC}. In addition, it would be possible to evaluate the fertilization requirements of the crop and the extent to which these have been met in line with N uptake. This may be accomplished by employing the aforementioned relationships through the f_{CC} of the images, initially obtaining DM and subsequently $\%N_{crit}$, with N uptake.

4.1.2. The Impact of Nitrogen Fertilization on Crop Response

Crop performance differed significantly across the three years of the trial, with 2020 being the most productive, both in terms of total above-ground biomass and yield. In 2020, the discrepancies between the experimental treatments with regard to biomass production were almost entirely mirrored in the yield of fruit, which remained relatively consistent despite the application of N fertilizer at rates ranging from 0 to 180 kg/ha of N. The mineral N present in the soil at the outset of the crop cycle was 177 kg/ha, and in conjunction with the mineralization of organic matter, it was sufficient to meet the N uptake, which ranged from 200 to 300 kg/ha. In the two subsequent years, the initial mineral N contents were 149 and 92 kg/ha, respectively, in 2021 and 2022. The greatest discrepancies in production between treatments were observed in 2022, when pepper in the N0 treatment exhibited overt indications of N deficiency and was the least productive. Although no N deficiencies in the treatments in 2021 and 2022 were found, their productivity remained inferior to that of the 2020 treatments. The initial leaf N concentration was lower in 2021 and 2022 than in 2020 (Figure 12), despite the soil mineral N content being sufficient to meet plant needs at these early stages. As illustrated in Figure 10, the highest yield of dry matter corresponded to fruits, which represent the most significant yield component. The interannual differences in production and flower set, in addition to a longer harvesting period in 2020, were responsible for the observed variations. In 2022, the temperature was exceedingly high, occurring concurrently with the peak flowering period, which may have negatively impacted flowering and fruit set. As posited by Van Eerd (2007) [70], the lack of yield response to N observed in sweet-pepper trials conducted in disparate locations can be partially attributed to the prevailing hot and dry climatic conditions, wherein humidity, rather than N, constitutes the most limiting growth factor. The conditions under which this study was conducted are representative of those typically found in the region. The grouping of ripening is an important aspect for processing peppers to reduce harvesting costs. While N0 treatment exhibited some advancement and greater clustering of fruit ripening, the differences observed between this treatment and the other treatments were minimal.

In the three-year trial period, the highest yields were obtained with N inputs equal to or less than 200 kg N/ha, which represents the maximum dose permitted in Extremadura by regulations for areas vulnerable to nitrate contamination [22]. Some sources recommend higher doses for outdoor bell pepper cultivation, exceeding the aforementioned limit. For instance, Zhang et al. (2023) [71] conducted experiments in China with an N input of 225 kg N/ha, while Kuşçu et al. (2016) [72] used 240 kg N/ha in Turkey. Hartz et al. (1993) [73] applied up to 252 kg N/ha in California. Nevertheless, lower doses have also been identified, ranging from 125 to 150 kg N/ha [8,74], with Sambo et al. (2004) [9] proposing 120 kg N/ha in alignment with the findings of this study. These findings underscore the necessity of integrating the mineralization of plant debris into the fertilization plan, in addition to the mineral N applied at the outset of the crop cycle. Tei et al. (2020) [75] highlighted this point by indicating, as can be seen in Figure 16, that at the moment of transplanting a mineralization process is initiated, which results in the excessive availability of mineralized N along the crop cycle, without the need to take advantage of the applications made.

Notwithstanding the fluctuations in yield observed in the course of the field experiments over time, the results consistently exceeded the regional average in Extremadura, which stands at approximately 45,000 kg/ha [76]. Moreover, these outcomes surpass the yield data documented by other researchers for industrial bell pepper cultivated under open-air conditions. In Turkey, the yield was 48,000 kg/ha [72], while in China it was 46,540 kg/ha [74].

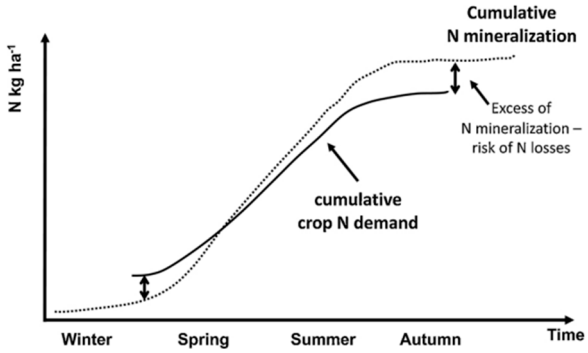

Figure 16. Increased mineralization throughout the year in response to crop N demand. Source: Tei et al. (2020) [75].

4.1.3. Crop N Uptake and Nutritional Status

The results obtained provide information of practical interest for the elaboration and readjustment of the N fertilization plan for an industrial bell pepper crop of this type. As illustrated in Figure 15, maximum fruit production is achieved with inputs of 200 kg N/ha, with higher inputs not resulting in higher yields. The uptake pattern is marked by the evolution of the above-ground biomass, which can be monitored by sensor-based techniques. Furthermore, the relationships obtained allow corrections to be made thanks to the modeling of industrial peppers grown in open fields.

A further aspect to consider in the context of fertilization plans is the characterization of nutritional status. In the case of N, foliar diagnosis requires specific observations. This element is subject to what is referred to as 'luxury consumption' [62]. In 2022, the most notable contrasts between treatments were observed in various parameters measured. However, the discrepancies in foliar N content between N1 and N2 were not sustained in fruit production. Conversely, when comparing the seasonal evolution of these foliar concentrations in 2020 and 2022, it is challenging to propose valid reference levels for both years. A more reliable reference point is the critical curve, which was maintained by all treatments in the 2020 and 2021 trials. This is consistent with the observed evolution of the same years. However, in 2022, the critical curve shows clear differences between treatments, indicating N0 as deficient and N2 as overfertilized, due to the more pronounced over-fertilization of N2 in this campaign. The diagnostic system is valid for applications involving the production of 1 tn/ha of aerial dry matter [37,57].

5. Conclusions

This article presents key relationships for monitoring outdoor processing-pepper crop growth, including vegetative development and CNC. These relationships help optimize fertilization in real time using satellite imagery or drones. In addition, this information will be useful for the adaptation of simulation models such as VegSyst to outdoor processing peppers.

Applying the information from this study to the conditions of Las Vegas del Guadiana, this paper shows that it is possible to reduce nitrate leaching and costs, since the best nitrogen doses were 120 kg N/ha, much lower than those commonly applied. In addition, lower nitrogen rates promote early ripening, which can reduce harvesting costs or facilitate mechanization.

Author Contributions: Conceptualization, J.M.V. and H.P.; methodology, J.M.V., H.P. and C.C.; software, J.M.V.; validation, J.M.V.; formal analysis, J.M.V.; investigation, J.M.V., C.C., V.G. and H.P.; resources, J.M.V., H.P., C.C. and V.G.; data curation, J.M.V.; writing—original draft preparation, J.M.V.; writing—review and editing, J.M.V., H.P.; visualization, J.M.V., C.C., V.G. and H.P.; supervision, H.P. and C.C.; project administration, C.C.; funding acquisition, C.C. All authors have read and agreed to the published version of the manuscript.

Funding: This research was funded by Junta de Extremadura, grant number PD18069. Project PDC2022-133936-I00 funded by the Ministry of Science, Innovation and Universities/State Research Agency/10.13039/501100011033 and by the European Union Next GenerationEU/Recovery, Transformation and Resilience Plan for Spain. Project RTI2018-095298 funded by funded by Ministerio de Ciencia, Innovación y Universidades/Agencia Estatal de Investigación/10.13039/501100011033/ and by FEDER A way of doing Europe.

Data Availability Statement: The original contributions presented in the study are included in the article, further inquiries can be directed to the corresponding author.

Acknowledgments: Eugenio Márquez is thanked for his technical work.

Conflicts of Interest: The authors declare no conflicts of interest.

References

1. MAPA (Ministerio de Agricultura, Pesca y Alimentación). Anuario de Estadística. Avance de Superficies y Producciones de Cultivo. Madrid, España. 2022. Available online: https://www.mapa.gob.es/es/estadistica/temas/publicaciones/anuario-de-estadistica/2023/default.aspx?parte=3&capitulo=07&grupo=6&seccion=27 (accessed on 8 July 2024). (In Spanish)
2. da Silva, J.M.; Fontes, P.C.R.; do Milagres, C.C.; de Abreu, J.A.A. Yield and nitrogen use efficiency of bell pepper grown in SLAB fertigated with different nitrogen rates. *J. Plant Nutr.* **2020**, *43*, 2833–2843. [CrossRef]
3. Flores, P.; Castellar, I.; Hellín, P.; Fenoll, J.; Navarro, J. Response of pepper plants to different rates of mineral fertilizers after soil biofumigation and solarization. *J. Plant Nutr.* **2007**, *30*, 367–379. [CrossRef]
4. Grasso, R.; de Souza, R.; Peña-Fleitas, M.T.; Gallardo, M.; Thompson, R.B.; Padilla, F.M. Root and crop responses of sweet pepper (*Capsicum annuum*) to increasing N fertilization. *Sci. Hortic.* **2020**, *273*, 109645. [CrossRef]
5. Medina-Lara, F.; Echevarría-Machado, I.; Pacheco-Arjona, R.; Ruiz-Lau, N.; Guzmán-Antonio, A.; Martinez-Estevez, M. Influence of nitrogen and potassium fertilization on fruiting and capsaicin content in habanero pepper (*Capsicum chinense* Jacq.). *HortScience* **2008**, *43*, 1549–1554. [CrossRef]
6. Rodríguez, A.; Peña-Fleitas, M.T.; Gallardo, M.; de Souza, R.; Padilla, F.M.; Thompson, R.B. Sweet pepper and nitrogen supply in greenhouse production: Critical nitrogen curve, agronomic responses and risk of nitrogen loss. *Eur. J. Agron.* **2020**, *117*, 126046. [CrossRef]
7. Yasuor, H.; Ben-Gal, A.; Yermiyahu, U.; Beit-Yannai, E.; Cohen, S. Nitrogen Management of Greenhouse Pepper Production: Agronomic, Nutritional, and Environmental Implications. *HortScience* **2013**, *48*, 1241–1249. [CrossRef]
8. Saqib, M.; Anjum, M.A.; Hoogenboom, G. The performance of sweet pepper cultivars under different nitrogen levels in a semi-arid environment. *J. Plant Nutr.* **2023**, *46*, 984–995. [CrossRef]
9. Sambo, P.; Borsato, D.; Gianquinto, G. Effect of Nitrogen Fertilization on Yield and Canopy Reflectance of Pepper (*Capsicum annuum*). *HortScience* **2004**, *39*, 871. [CrossRef]
10. Ladha, J.K.; Jat, M.L.; Stirling, C.M.; Chakraborty, D.; Pradhan, P.; Krupnik, T.J.; Sapkota, T.B.; Pathak, H.; Rana, D.S.; Tesfaye, K.; et al. Achieving the sustainable development goals in agriculture: The crucial role of nitrogen in cereal-based systems. *Adv. Agron.* **2020**, *163*, 39–116. [CrossRef]
11. Ata-Ul-Karim, S.T.; Cang, L.; Wang, Y.; Zhou, D. Effects of soil properties, nitrogen application, plant phenology, and their interactions on plant uptake of cadmium in wheat. *J. Hazard. Mater.* **2020**, *384*, 121452. [CrossRef]
12. Evans, J.R.; Clarke, V.C. The nitrogen cost of photosynthesis. *J. Exp. Bot.* **2019**, *70*, 7–15. [CrossRef] [PubMed]
13. Thompson, R.B.; Martínez-Gaitan, C.; Gallardo, M.; Giménez, C.; Fernández, M.D. Identification of irrigation and N management practices that contribute to nitrate leaching loss from an intensive vegetable production system by use of a comprehensive survey. *Agric. Water Manag.* **2007**, *89*, 261–274. [CrossRef]
14. Li, P.; Karunanidhi, D.; Subramani, T.; Srinivasamoorthy, K. Sources and Consequences of Groundwater Contamination. *Arch. Environ. Contam. Toxicol.* **2021**, *80*, 1–10. [CrossRef] [PubMed]
15. Galloway, J. The global nitrogen cycle: Changes and consequences—All Databases. *Environ. Pollut.* **1998**, *102*, 15–24. [CrossRef]
16. Li, X.; Ata-UI-Karim, S.T.; Li, Y.; Yuan, F.; Miao, Y.; Yoichiro, K.; Cheng, T.; Tang, L.; Tian, X.; Liu, X.; et al. Advances in the estimations and applications of critical nitrogen dilution curve and nitrogen nutrition index of major cereal crops. A review. *Comput. Electron. Agric.* **2022**, *197*, 106998. [CrossRef]
17. Jaworska, G. Content of nitrates, nitrites, and oxalates in New Zealand spinach. *Food Chem.* **2005**, *89*, 235–242. [CrossRef]
18. Vega-Castellote, M.; Pérez-Marín, D.; Torres, I.; Sánchez, M.T. Online NIRS analysis for the routine assessment of the nitrate content in spinach plants in the processing industry using linear and non-linear methods. *LWT* **2021**, *151*, 112192. [CrossRef]
19. Neeteson, J.J. Look at it this way. *Outlook Agric.* **1994**, *23*, 3–4. [CrossRef]
20. Zhan, Y.; Guo, Z.; Ruzzante, S.; Gleeson, T.; Andrews, C.B.; Babovic, V.; Zheng, C. Assessment of spatiotemporal risks for nationwide groundwater nitrate contamination. *Sci. Total Environ.* **2024**, *947*, 174508. [CrossRef]
21. Fereres, E.; Goldhamer, D.A.; Parsons, L.R. Irrigation water management of horticultural crops. *HortScience* **2003**, *38*, 1036–1042. [CrossRef]

22. Directive Council. Concerning the protection of waters against pollution caused by nitrates from agricultural sources. *Off. J. L* **1991**, *375*, 1–8.
23. Thompson, R.B.; Incrocci, L.; Voogt, W.; Pardossi, A.; Magán, J.J. Sustainable irrigation and nitrogen management of fertigated vegetable crops. *Acta Hortic.* **2017**, *1150*, 363–378. [CrossRef]
24. Biernbaum, J.A. Root-zone Management of Greenhouse Container-grown Crops to Control Water and Fertilizer. *HortTechnology* **1992**, *2*, 127–132. [CrossRef]
25. Pan, Y.; She, D.; Ding, J.; Abulaiti, A.; Zhao, J.; Wang, Y.; Liu, R.; Wang, F.; Shan, J.; Xia, Y. Coping with groundwater pollution in high-nitrate leaching areas: The efficacy of denitrification. *Environ. Res.* **2024**, *250*, 118484. [CrossRef] [PubMed]
26. Zhu, J.H.; Li, X.L.; Christie, P.; Li, J.L. Environmental implications of low nitrogen use efficiency in excessively fertilized hot pepper (*Capsicum frutescens* L.) cropping systems. *Agric. Ecosyst. Environ.* **2005**, *111*, 70–80. [CrossRef]
27. Chojnacka, K.; Mikula, K.; Skrzypczak, D.; Izydorczyk, G.; Gorazda, K.; Kulczycka, J.; Kominko, H.; Moustakas, K.; Witek-Krowiak, A. Practical aspects of biowastes conversion to fertilizers. *Biomass Convers. Biorefinery* **2022**, *1*, 1515–1533. [CrossRef]
28. Larsen, R.; International Society for Horticultural Science. Section Vegetables; ISHS Working Group on Vegetable Nutrition and Fertilization. In Proceedings of the IVth International Symposium on Ecologically Sound Fertilization Strategies for Field Vegetable Production, Malmo, Sweden, 22–25 September 2008.
29. MacHet, J.M.; Dubrulle, P.; Damay, N.; Duval, R.; Julien, J.L.; Recous, S. A dynamic decision-making tool for calculating the optimal rates of N application for 40 annual crops while minimising the residual level of mineral N at harvest. *Agronomy* **2017**, *7*, 73. [CrossRef]
30. Feller, C. N-Expert—Fertiliser Recommendations for Field Vegetables. Available online: https://n-expert.igzev.de/ (accessed on 16 December 2022).
31. Gallardo, M.; Fernández, M.D.; Giménez, C.; Padilla, F.M.; Thompson, R.B. Revised VegSyst model to calculate dry matter production, critical N uptake and ETc of several vegetable species grown in Mediterranean greenhouses. *Agric. Syst.* **2016**, *146*, 30–43. [CrossRef]
32. Gallardo, M.; Thompson, R.B.; Giménez, C.; Padilla, F.M.; Stöckle, C.O. Prototype decision support system based on the VegSyst simulation model to calculate crop N and water requirements for tomato under plastic cover. *Irrig. Sci.* **2014**, *32*, 237–253. [CrossRef]
33. Gallardo, M.; Giménez, C.; Martínez-Gaitán, C.; Stöckle, C.O.; Thompson, R.B.; Granados, M.R. Evaluation of the VegSyst model with muskmelon to simulate crop growth, nitrogen uptake and evapotranspiration. *Agric. Water Manag.* **2011**, *101*, 107–117. [CrossRef]
34. Gallardo, M.; Gimenez, C.; Fernández, M.D.; Padilla, F.M.; Thompson, R.B. Use of the VegSyst model to calculate crop N uptake and crop evapotranspiration of autumn- and spring-grown cucumber in Mediterranean greenhouses. In Proceedings of the Acta Horticulturae, Wageningen, The Netherlands, 15 March 2017; International Society for Horticultural Science: Leuven, Belgium, 2017; Volume 1154, pp. 47–54.
35. Giménez, C.; Gallardo, M.; Martínez-Gaitán, C.; Stöckle, C.O.; Thompson, R.B.; Granados, M.R. VegSyst, a simulation model of daily crop growth, nitrogen uptake and evapotranspiration for pepper crops for use in an on-farm decision support system. *Irrig. Sci.* **2013**, *31*, 465–477. [CrossRef]
36. Giménez, C.; Thompson, R.B.; Prieto, M.H.; Suárez-Rey, E.; Padilla, F.M.; Gallardo, M. Adaptation of the VegSyst model to outdoor conditions for leafy vegetables and processing tomato. *Agric. Syst.* **2019**, *171*, 51–64. [CrossRef]
37. Justes, E.; Mary, B.; Meynard, J.M.; Machet, J.M.; Thelier-Huche, L. Determination of a Critical Nitrogen Dilution Curve for Winter Wheat Crops. *Ann. Bot.* **1994**, *74*, 397–407. [CrossRef]
38. Fu, Z.; Zhang, J.; Jiang, J.; Zhang, Z.; Cao, Q.; Tian, Y.; Zhu, Y.; Cao, W.; Liu, X. Using the time series nitrogen diagnosis curve for precise nitrogen management in wheat and rice. *Field Crop. Res.* **2024**, *307*, 109259. [CrossRef]
39. Huang, S.; Miao, Y.; Cao, Q.; Yao, Y.; Zhao, G.; Yu, W.; Shen, J.; Yu, K.; Bareth, G. A New Critical Nitrogen Dilution Curve for Rice Nitrogen Status Diagnosis in Northeast China. *Pedosphere* **2018**, *28*, 814–822. [CrossRef]
40. Song, L.; Wang, S.; Ye, W. Establishment and application of critical nitrogen dilution curve for rice based on leaf dry matter. *Agronomy* **2020**, *10*, 367. [CrossRef]
41. Yue, S.C.; Sun, F.L.; Meng, Q.F.; Zhao, R.F.; Li, F.; Chen, X.P.; Zhang, F.S.; Cui, Z.L. Validation of a Critical Nitrogen Curve for Summer Maize in the North China Plain. *Pedosphere* **2014**, *24*, 76–83. [CrossRef]
42. Li, W.; Gu, X.; Fang, H.; Zhao, T.; Yin, R.; Cheng, Z.; Tan, C.; Zhou, Z.; Du, Y. Optimizing nitrogen application rate by establishing a unified critical nitrogen dilution curve for maize under different mulching planting patterns. *Eur. J. Agron.* **2024**, *152*, 127026. [CrossRef]
43. Abdallah, F.B.; Olivier, M.; Goffart, J.P.; Minet, O. Establishing the Nitrogen Dilution Curve for Potato Cultivar Bintje in Belgium. *Potato Res.* **2016**, *59*, 241–258. [CrossRef]
44. Giletto, C.M.; Echeverría, H.E. Critical Nitrogen Dilution Curve for Processing Potato in Argentinean Humid Pampas. *Am. J. Potato Res.* **2012**, *89*, 102–110. [CrossRef]
45. Tei, F.; Benincasa, P.; Guiducci, M. Critical nitrogen concentration in processing tomato. *Eur. J. Agron.* **2002**, *18*, 45–55. [CrossRef]
46. Padilla, F.M.; Peña-Fleitas, M.T.; Gallardo, M.; Thompson, R.B. Threshold values of canopy reflectance indices and chlorophyll meter readings for optimal nitrogen nutrition of tomato. *Ann. Appl. Biol.* **2015**, *166*, 271–285. [CrossRef]

47. Padilla, F.M.; Peña-Fleitas, M.T.; Gallardo, M.; Giménez, C.; Thompson, R.B. Derivation of sufficiency values of a chlorophyll meter to estimate cucumber nitrogen status and yield. *Comput. Electron. Agric.* **2017**, *141*, 54–64. [CrossRef]
48. Soil Survey Staff. Soil Taxonomy. In *A Basic System of Soil Classification for Making and Interpreting Soil Surveys*; United States Department of Agriculture, Natural Resources Conservation Service: Washington, DC, USA, 1999.
49. Board, J.E.; Kamal, M.; Harville, B.G. Temporal Importance of Greater Light Interception to Increased Yield in Narrow-Row Soybean. *Agron. J.* **1992**, *84*, 575–579. [CrossRef]
50. Egli, D.B. Mechanisms responsible for soybean yield response to equidistant planting patterns. *Agron. J.* **1994**, *86*, 1046–1049. [CrossRef]
51. Campillo, C.; Prieto, M.H.; Daza, C.; Moñino, M.J.; García, M.I. Using digital images to characterize canopy coverage and light interception in a processing tomato crop. *HortScience* **2008**, *43*, 1780–1786. [CrossRef]
52. Kiniry, J.; Johnson, M.V.; Mitchell, R.; Vogel, K.; Kaiser, J.; Bruckerhoff, S.; Cordsiemon, R. Switchgrass Leaf Area Index and Light Extinction Coefficients. *Agron. J.* **2011**, *103*, 119–122. [CrossRef]
53. Lacasa, J.; Hefley, T.J.; Otegui, M.E.; Ciampitti, I.A. A Practical Guide to Estimating the Light Extinction Coefficient with Nonlinear Models—A Case Study on Maize. *Plant Methods* **2021**, *17*, 60. [CrossRef]
54. Monsi, M.; Saeki, T.; Schortemeyer, M. On the factor light in plant communities and its importance for matter production. *Ann. Bot.* **2005**, *95*, 549–567. [CrossRef]
55. Greenwood, D.J.; Lemaire, G.; Gosse, G.; Cruz, P.; Draycott, A.; Neeteson, J.J. Decline in percentage N of C3 and C4 crops with increasing plant mass. *Ann. Bot.* **1990**, *66*, 425–436. [CrossRef]
56. Padilla, F.M.; Peña-Fleitas, M.T.; Gallardo, M.; Thompson, R.B. Proximal optical sensing of cucumber crop N status using chlorophyll fluorescence indices. *Eur. J. Agron.* **2016**, *73*, 83–97. [CrossRef]
57. Ziadi, N.; Bélanger, G.; Claessens, A.; Lefebvre, L.; Cambouris, A.N.; Tremblay, N.; Nolin, M.C.; Parent, L.É. Determination of a critical nitrogen dilution curve for spring wheat. *Agron. J.* **2010**, *102*, 241–250. [CrossRef]
58. Sempere, A.; Oliver, J.; Ramos, C. Simple determination of nitrate in soils by second-derivative spectroscopy. *J. Soil Sci.* **1993**, *44*, 633–639. [CrossRef]
59. Rhine, E.D.; Mulvaney, R.L.; Pratt, E.J.; Sims, G.K. Improving the Berthelot Reaction for Determining Ammonium in Soil Extracts and Water. *Soil Sci. Soc. Am. J.* **1998**, *62*, 473–480. [CrossRef]
60. Marcelis, L.F.M.; Elings, A.; Dieleman, J.A.; De Visser, P.H.B.; Brajeul, E.; Bakker, M.J.; Heuvelink, E. Modelling dry matter production and partitioning in sweet pepper. *Acta Hortic.* **2006**, *718*, 121–128. [CrossRef]
61. Lemaire, G.; Gastal, F. N Uptake and Distribution in Plant Canopies. In *Diagnosis of the Nitrogen Status in Crops*; Springer: Berlin/Heidelberg, Germany, 1997; pp. 3–43. [CrossRef]
62. Zhang, J.; Blackmer, A.M.; Ellsworth, J.W.; Kyveryga, P.M.; Blackmer, T.M. Luxury Production of Leaf Chlorophyll and Mid-Season Recovery from Nitrogen Deficiencies in Corn. *Agron. J.* **2008**, *100*, 658–664. [CrossRef]
63. Tang, R.; Supit, I.; Hutjes, R.; Zhang, F.; Wang, X.; Chen, X.; Zhang, F.; Chen, X. Modelling growth of chili pepper (*Capsicum annuum* L.) with the WOFOST model. *Agric. Syst.* **2023**, *209*, 103688. [CrossRef]
64. Mercado-Luna, A.; Rico-García, E.; Lara-Herrera, A.; Soto-Zarazúa, G.; Ocampo-Velázquez, R.; Guevara-González, R.; Herrera-Ruiz, G.; Torres-Pacheco, I. Nitrogen determination on tomato (*Lycopersicon esculentum* Mill.) seedlings by color image analysis (RGB). *Afr. J. Biotechnol.* **2010**, *9*, 5326–5332.
65. Yuzhu, H.; Xiaomei, W.; Shuyao, S. Nitrogen determination in pepper (*Capsicum frutescens* L.) plants by color image analysis (RGB). *Afr. J. Biotechnol.* **2011**, *10*, 17737–17741. [CrossRef]
66. Lukina, E.V.; Stone, M.L.; Raun, W.R. Estimating vegetation coverage in wheat using digital images. *J. Plant Nutr.* **1999**, *22*, 341–350. [CrossRef]
67. Gastal, F.; Lemaire, G. N uptake and distribution in crops: An agronomical and ecophysiological perspective. *J. Exp. Bot.* **2002**, *53*, 789–799. [CrossRef] [PubMed]
68. Lemaire, G.; Jeuffroy, M.H.; Gastal, F. Diagnosis tool for plant and crop N status in vegetative stage. Theory and practices for crop N management. *Eur. J. Agron.* **2008**, *28*, 614–624. [CrossRef]
69. Seginer, I. Plant spacing effect on the nitrogen concentration of a crop. *Eur. J. Agron.* **2004**, *21*, 369–377. [CrossRef]
70. Van Eerd, L.L. Evaluation of different nitrogen use efficiency indices using field-grown green bell peppers (*Capsicum annuum* L.). *Can. J. Plant Sci.* **2007**, *87*, 565–569. [CrossRef]
71. Zhang, H.; Wang, Y.; Yu, S.; Zhou, C.; Li, F.; Chen, X.; Liu, L.; Wang, Y. Plant Photosynthesis and Dry Matter Accumulation Response of Sweet Pepper to Water–Nitrogen Coupling in Cold and Arid Environment. *Water* **2023**, *15*, 2134. [CrossRef]
72. Kuşçu, H.; Turhan, A.; Özmen, N.; Aydınol, P.; Demir, A.O. Response of red pepper to deficit irrigation and nitrogen fertigation. *Arch. Agron. Soil Sci.* **2016**, *62*, 1396–1410. [CrossRef]
73. Hartz, T.K.; LeStrange, M.; May, D.M. Nitrogen Requirements of Drip-irrigated Peppers. *HortScience* **1993**, *28*, 1097–1099. [CrossRef]
74. Kong, Q.; Li, G.; Wang, Y.; Huo, H. Bell pepper response to surface and subsurface drip irrigation under different fertigation levels. *Irrig. Sci.* **2012**, *30*, 233–245. [CrossRef]

75. Tei, F.; De Neve, S.; de Haan, J.; Kristensen, H.L. Nitrogen management of vegetable crops. *Agric. Water Manag.* **2020**, *240*, 106316. [CrossRef]
76. MAPA (Ministerio de Agricultura, Pesca y Alimentación); Spanish National Goverment. Anuario de Estadística. 2021. Available online: https://www.mapa.gob.es/es/estadistica/temas/publicaciones/anuario-de-estadistica/2021/default.aspx?parte=3&capitulo=07&grupo=6 (accessed on 4 September 2023).